Journal of Power Sources 213 (2012) 270–274

Contents lists available at SciVerse ScienceDirect

Journal of Power Sources

journal homepage: www.elsevier.com/locate/jpowsour

Short communication

Enhanced oxygen diffusion in low barium-containing $La_{0.2175}Pr_{0.2175}Ba_{0.145}Sr_{0.4}Fe_{0.8}Co_{0.2}O_{3-\delta}$ intermediate temperature solid oxide fuel cell cathodes

Vicente B. Vert [a], José M. Serra [a], John A. Kilner [b], Mónica Burriel [b,*]

[a] Instituto de Tecnología Química, Universitat Politècnica de València, Consejo Superior de Investigaciones Científicas, Av. Los Naranjos, s/n, 46022 Valencia, Spain
[b] Department of Materials, Imperial College London, Exhibition Road, London SW7 2AZ, United Kingdom

ARTICLE INFO

Article history:
Received 26 January 2012
Received in revised form
16 April 2012
Accepted 18 April 2012
Available online 26 April 2012

keywords:
Time-of-flight secondary ion mass spectrometry (ToF-SIMS)
Intermediate temperature solid oxide fuel cells (IT-SOFC)
Cathodes
Perovskite
Oxygen diffusion
Surface exchange

ABSTRACT

Isotopic tracer diffusion studies have been performed on the perovskite composition $La_{0.2175}Pr_{0.2175}Ba_{0.145}Sr_{0.4}Fe_{0.8}Co_{0.2}O_{3-\delta}$ to obtain the diffusion and surface exchange coefficients for oxygen. This material has been identified as a highly active electrocatalytic cathode for intermediate temperature solid oxide fuel cells. The oxygen diffusion coefficients obtained in the 450–650 °C temperature range are higher than the ones measured for most of the cathode materials reported in the literature and they agree with those calculated from electrochemical impedance spectroscopy measurements performed on symmetrical cells.

1. Introduction

Solid oxide fuel cells (SOFCs) are nearing the end of their development phase, however, there are still significant problems to be overcome concerning cost reduction and long term durability before full commercialisation can be achieved. A reduction of the operating temperature of the device is one way to ameliorate these problems, most of which are exacerbated by the very high temperatures (circa 1000 °C) of earlier generations of SOFCs. When decreasing the operation temperature below 700 °C (often known as Intermediate Temperature SOFCs or IT-SOFCs), the performance of the SOFCs seems to be critically influenced by the cathode electrochemical characteristics [1] and thus new, active cathode materials are needed to retain high performance at these lower temperatures. One approach to the discovery of new materials is by combinatorial methods and, in an earlier work, some multi-element compositions with electrode resistances several orders of magnitude lower than $La_{0.58}Sr_{0.4}Fe_{0.8}Co_{0.2}O_{3-\delta}$ (LSFC) [2] were discovered with rather low apparent activation energies. These new multi-element cathodes, namely the $(La–Pr–Sm–Ba)_{0.58}Sr_{0.4}Fe_{0.8}Co_{0.2}O_{3-\delta}$ system, combine, on the same lattice, lanthanum, praseodymium, samarium and/or barium with strontium, iron and cobalt. The multi-element compositions with the lowest cathode polarization resistance had comparatively high oxygen diffusion and surface exchange coefficients, as shown by the parameters obtained from electrochemical impedance spectroscopy (EIS) modelling [3].

In this work, the oxygen transport parameters estimated by EIS on the $La_{0.2175}Pr_{0.2175}Ba_{0.145}Sr_{0.4}Fe_{0.8}Co_{0.2}O_{3-\delta}$ composition have been compared with those obtained by means of oxygen isotopic exchange measurements and SIMS depth profiling using Time-of-Flight Secondary Ion Mass Spectrometry (ToF-SIMS) analysis.

2. Experimental

Sintered ~3 mm thick pellets made of pressed $La_{0.2175}Pr_{0.2175}Ba_{0.145}Sr_{0.4}Fe_{0.8}Co_{0.2}O_{3-\delta}$ perovskite powders were obtained after calcination at 1300 °C for 12 h. The initial powder was obtained by the Pechini method [4] after calcination at 1000 °C. Phase purity was checked by X-Ray diffraction in a PAN'Alytical CUBIX equipment. Secondary Electron Microscopy (SEM) imaging was performed on a JEOL JSM6300 microscope.

* Corresponding author. Tel.: +44 (0)20 7594 6771; fax: +44 (0)20 7594 6757.
E-mail address: m.burriel@imperial.ac.uk (M. Burriel).

0378-7753/$ – see front matter © 2012 Elsevier B.V. All rights reserved.
doi:10.1016/j.jpowsour.2012.04.041

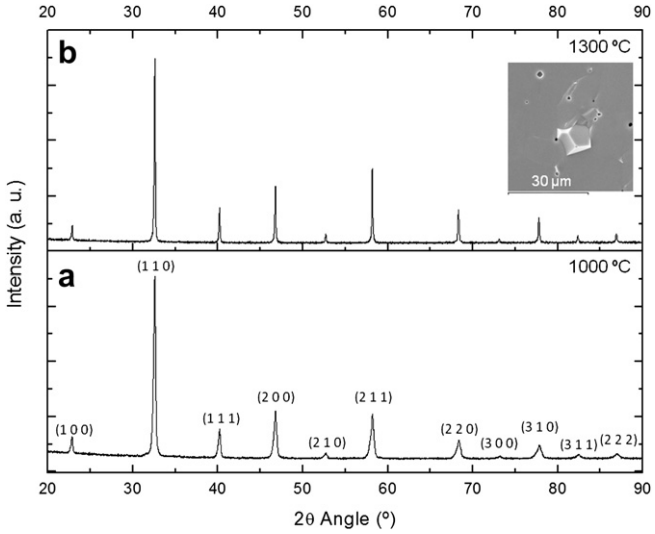

Fig. 1. Powder XRD pattern of the LPBSFC perovskite showing a pure cubic single phase (peaks indexed) both after synthesising at 1000 °C (a) and after densification at 1300 °C (b). A SEM image of a cross-section of a dense pellet is shown in the inset.

Clean sintered samples polished down to a 0.25 μm finish were placed in a quartz tube for the oxygen isotopic exchange. The description of the exchange rig, the Isotope Exchange Depth Profile (IEDP) method and the sample preparation can be found in Ref. [5–8]. Prior to the ^{18}O exchange the samples were pre-annealed in research grade oxygen $^{16}O_2$ (99.9995%) at high temperature (900 °C) for 2 h and then under the same conditions as the subsequent isotopic exchange (450–650 °C temperature range). In all cases the water vapour content of the oxygen gas used was very low (~1 to 2 vppm).

Time-of-Flight SIMS analyses have been carried out on an Ion ToF-SIMS 5 machine (ION-TOF GmbH, Münster, Germany) by using a Bi^+ Liquid Metal Ion Gun (LMIG) primary gun (2 kV) and a Cs^+ second ion gun for sputter removal. The data were obtained by burst-mode operation with eight peaks and measuring the negative secondary ion mass spectrum. ToF-SIMS data analysis was performed using ION-TOF software.

3. Results and discussion

In spite of the number of elements present in the $La_{0.2175}Pr_{0.2175}Ba_{0.145}Sr_{0.4}Fe_{0.8}Co_{0.2}O_{3-\delta}$ material (hereinafter abbreviated as LPBSFC), a single cubic perovskite phase can be obtained after a firing step at 1000 °C, as shown in the diffraction pattern in Fig. 1a. Furthermore, after densification at 1300 °C, the same perovskite structure is still maintained (Fig. 1b). The XRD pattern in Fig. 1b has been obtained from sintered pellets which were subsequently pulverised for the X-ray measurement. The narrower diffraction peaks obtained after the higher-temperature treatment can be attributed to the presence of larger grains. LPBSFC showed high temperature structural stability since no other phase-related peaks appeared after heating to 1300 °C (Fig. 1b). In addition, it was possible to obtain very dense samples of LPBSFC material, as can be seen in the SEM cross-section image of sintered pellets (inset in Fig. 1b). Thus this material could also be fabricated, for instance, as a membrane for oxygen separation [9]. The density of the bulk material is high enough to allow measurement by the isotopic exchange technique despite to the fact that these samples possess some closed porosity (<3 μm in diameter).

In order to measure the exchange and diffusion properties of the LPBSFC material $^{18}O_2/^{16}O_2$ exchanges were carried out at five different temperatures in the 450–650 °C range on polished dense samples. The samples were then cut into half and the cut faces normal to the original surface were polished prior to SIMS analysis. The secondary ion signals for all the elements of the $La_{0.2175}Pr_{0.2175}Ba_{0.145}Sr_{0.4}Fe_{0.8}Co_{0.2}O_{3-\delta}$ material were monitored (as XO^- ions), in addition to the $^{18}O^-$ and $^{16}O^-$ signals. By using the imaging method, sampling large areas and delimiting the $^{18}O^-$ concentration profile calculation to pore-free regions, the influence of closed porosity has been excluded. As an illustration of a typical oxygen diffusion profile in a LPBSFC pellet, the $^{18}O^-$ surface map measured for the sample exchanged at 553 °C for 1576 s is shown in Fig. 2a. From these maps, and the corresponding maps for the $^{16}O^-$ signal, normalised isotopic fraction depth profiles can be readily obtained. By fitting these measured and normalised isotopic concentration profiles to the solution to the diffusion equation for a semi-infinite solid [10] (Eq. (1)), the oxygen tracer diffusion (D^*) and surface exchange (k^*) coefficients can be obtained:

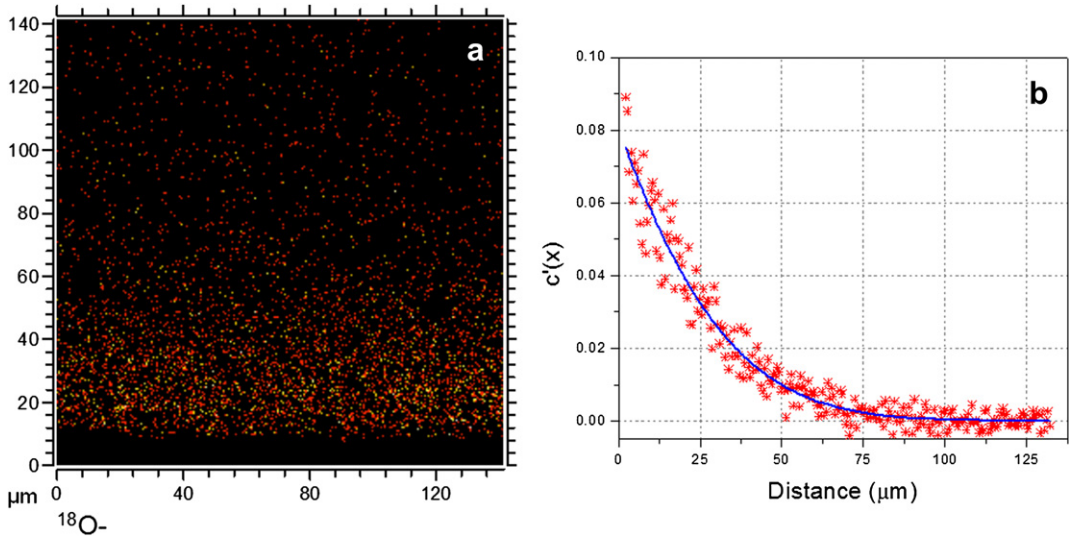

Fig. 2. (a) A false colour ^{18}O surface map of a selected pore-free region for the LPBSFC sample exchanged at 553 °C. The original surface exposed to the $^{18}O_2$ gas is shown at the lower part of the diagram at height of ~10 μm. (b) A normalised ^{18}O depth profile obtained from the same sample. The solid line is a best fit to Eq. (1).

$$c'(x) = \mathrm{erfc}\left(\frac{x}{2\sqrt{D^* t}}\right) - \exp\left(\frac{k^* x}{D^*} + \frac{k^{*2} t}{D^*}\right) \times \mathrm{erfc}\left(\frac{x}{2\sqrt{D^* t}} + k^* \sqrt{\frac{t}{D^*}}\right) \quad (1)$$

where $c'(x)$ is the normalized ^{18}O isotopic concentration calculated from:

$$c'(x) = \frac{c^*(x) - c^*_{bg}}{c^*_g - c^*_{bg}} \quad (2)$$

where c^* is the ^{18}O fraction, c^*_{bg} is the natural $^{18}O_2$ isotopic (background) abundance (0.2%) and c^*_g is the $^{18}O_2$ gas isotopic fraction (24.4%) measured on a clean Si-surface which had been previously oxidised in the $^{18}O_2$ enriched-gas. As described in Ref. [5] the ^{18}O fraction c^* was calculated as:

$$c^* = \frac{[^{18}O]}{[^{18}O] + [^{16}O]} = \frac{\sum_i^k N_i^{18}}{\sum_i^k N_i^{18} + kN_1^{16}} \quad (3)$$

where N_i^M is the number of counts contained within the ith peak of the k ^{M}O burst peaks (k was set to 8). The correction presented in Ref. [11] has been used for the isotopic exchange time calculation. After fitting the normalised ^{18}O profile data obtained from the ToF-SIMS measurements on the treated samples, the oxygen tracer diffusion (D^*) and surface exchange (k^*) coefficients for each temperature have been calculated. The D^* and k^* values obtained for each one of the measured regions on the exchanged samples are detailed in Table 1 together with the temperatures and exchange times used for the IEDP experiments. As an example, for the sample exchanged at 553 °C the normalised ^{18}O profile of a pore-free selected region and its fit to the solution to the diffusion equation are plotted together in Fig. 2b, from which a D^* value of 5.52×10^{-9} cm^2 s^{-1} and a k^* value of 1.30×10^{-7} cm^2 s^{-1} were determined. In Fig. 3 the D^* and k^*obtained values for the LPBSFC material (inverted solid triangles (cyan)) are plotted together with literature values for other state-of-the-art cathode materials, also obtained by the Isotope Exchange Depth Profile (IEDP) technique. For simplicity at each temperature the mean D^* and k^* values have been plotted together with their error bars taking into account the values obtained for all the measured areas.

Fig. 3a shows that the diffusion coefficient D^* values for LPBSFC fit well to a linear slope in the Arrhenius plot with an activation energy of 1.41 ± 0.17 eV, which confirms the accuracy of the diffusivity values. The diffusion coefficients obtained for this multi-element material are higher than most of the previously studied materials, i.e., $La_{0.6}Sr_{0.4}Fe_{0.8}Co_{0.2}O_{3-\delta}$ (LSFC) [12], $La_{0.6}Sr_{0.4}CoO_{3-\delta}$ (LSC) [13], $La_2NiO_{4+\delta}$ (LNO) [14] and $GdBaCo_2O_{5+\delta}$ (GBCO) [15] and they are comparable to those reported for $Ba_{0.5}Sr_{0.5}Co_{0.8}Fe_{0.2}O_{3-\delta}$ (BSCF) [16] and $PrBaCo_2O_{5+\delta}$ (PBCO) [17] materials (Fig. 3a). The large diffusivity values of $La_{0.2175}Pr_{0.2175}Ba_{0.145}Sr_{0.4}Fe_{0.8}Co_{0.2}O_{3-\delta}$ with respect to $La_{0.6}Sr_{0.4}Co_{0.2}Fe_{0.8}O_{3-\delta}$ [12] (its parent compound) may be related to (i) a higher oxygen vacancy concentration, (ii) higher oxygen vacancy mobility related to larger lattice parameter [3] or (iii) to the formation of new transport paths with a lower migration energy [18].

However the k^* values present quite a large scatter (Fig. 3b) showing values comparable to other cathode materials [12–17] for the temperatures 482 and 553 °C, but much lower values for the other three temperatures 458, 600 and 646 °C. Scatter in the surface exchange coefficient measurements is rather common, as the oxygen exchange rate strongly depends on the chemical state of the outermost layer of the material, and this can be influenced by the history of the sample and by the equilibrium state at each temperature. To date the factors governing the oxygen exchange behaviour are not well understood. In order to elucidate the origin of the differences further work and surface specific experiments are in progress.

In a previous publication [3] LPBSFC was identified as a material with a high electrocatalytic activity for oxygen reduction, due to the relatively high oxygen surface exchange and diffusion coefficients. These results were based on the values obtained from modelling the electrochemical impedance spectroscopy measurements, performed on the same LPBSFC electrode material, and extracting the Gerischer parameters (k_G and Z_0) [3]. These pseudo-coefficients calculated in Ref. [3] cannot be taken as absolute oxygen surface exchange and diffusion coefficients, but they served for a qualitative comparison between materials.

It is possible, however, to make a quantitative comparison of the diffusion and surface exchange coefficients obtained in this work from the IEDP measurements with those obtained in the previous work [3] by using the definition of the Gerischer parameters[1] given in Ref. [19]. The parameters derived from the EIS modelling were obtained from a porous LPBSFC cathode applied on both sides of a dense $Ce_{0.8}Gd_{0.2}O_{2-x}$ electrolyte and sintered at 1060 °C for 2 h. To obtain values of the porosity (ε), tortuosity (τ), surface area density (A), thermodynamic factor (Γ) and oxygen ion and vacancy concentration[2] (c_i and c_v) for LPBSFC it was assumed that these would be the same as the mean values for the closely related $La_{0.58}Sr_{0.4}Co_{0.2}Fe_{0.8}O_{3-\delta}$ perovskite material given in Ref. [20], due to the fact that the sintering conditions, oxygen stoichiometry and fabrication procedure are almost the same. These oxygen ion diffusion and surface exchange coefficients (D_i and k_i) calculated from the EIS fitting can be directly compared to the IEDP-tracer ($D^*$and k^*) coefficients [21] since LPBSFC is an electron-rich perovskite material [22,23], and they are shown in Fig. 3.

Both the EIS-derived oxygen ion diffusion and surface exchange coefficients are slightly different to those obtained from the IEDP experiments (normal (blue) and inverted (cyan) triangles in Fig. 3, respectively), with the difference for the surface exchange coefficient, k, being the most marked. The possible reasons for this larger difference for k could be due to a number of factors. All the geometric and lattice parameters have been taken from the literature [20] and correspond, as previously indicated, to mean values for the composition $La_{0.58}Sr_{0.4}Co_{0.2}Fe_{0.8}O_{3-\delta}$ (which is, in fact, the parent composition for $La_{0.2175}Pr_{0.2175}Ba_{0.145}Sr_{0.4}Fe_{0.8}Co_{0.2}O_{3-\delta}$ with A-site substitution) and are hence thought to be reliable. As a simplification the thermodynamic factor, oxygen ion and vacancy concentration (pO_2-dependent parameters) have been kept constant with temperature over this limited temperature regime.

Table 1
Oxygen diffusion and surface exchange coefficients obtained from the fit (including uncertainties) for all the areas measured together with the temperatures and exchange times used for each of IEDP experiment.

Temperature (°C)	Exchange time (s)	D^* (cm^2 s^{-1})	k^* (cm s^{-1})
458	3448	$1.54 \pm 1.08 \times 10^{-11}$	$5.47 \pm 1.44 \times 10^{-10}$
		$2.04 \pm 0.80 \times 10^{-10}$	$1.03 \pm 0.15 \times 10^{-9}$
482	1717	$7.73 \pm 0.85 \times 10^{-10}$	$8.10 \pm 0.34 \times 10^{-8}$
		$1.02 \pm 0.08 \times 10^{-9}$	$1.10 \pm 0.03 \times 10^{-7}$
		$9.00 \pm 0.81 \times 10^{-10}$	$1.20 \pm 0.04 \times 10^{-7}$
		$9.12 \pm 1.48 \times 10^{-10}$	$1.32 \pm 0.08 \times 10^{-7}$
553	1576	$5.52 \pm 0.61 \times 10^{-9}$	$1.30 \pm 0.05 \times 10^{-7}$
600	1574	$1.07 \pm 0.57 \times 10^{-8}$	$1.01 \pm 0.20 \times 10^{-8}$
		$1.30 \pm 0.17 \times 10^{-8}$	$2.79 \pm 0.14 \times 10^{-8}$
646	727	$2.82 \pm 1.15 \times 10^{-8}$	$2.56 \pm 0.39 \times 10^{-8}$

[1] $k_G = (\Gamma A k_i c_i)/((1-\varepsilon)c_v)$ and $Z_0 = (RT)/(2c_i F^2)\sqrt{(\Gamma \tau c_i)/((1-\varepsilon)c_v D_i)}$.
[2] $c_v = c_{mc} - c_o$ and $c_i = c_o$ with the nomenclature defined in [20].

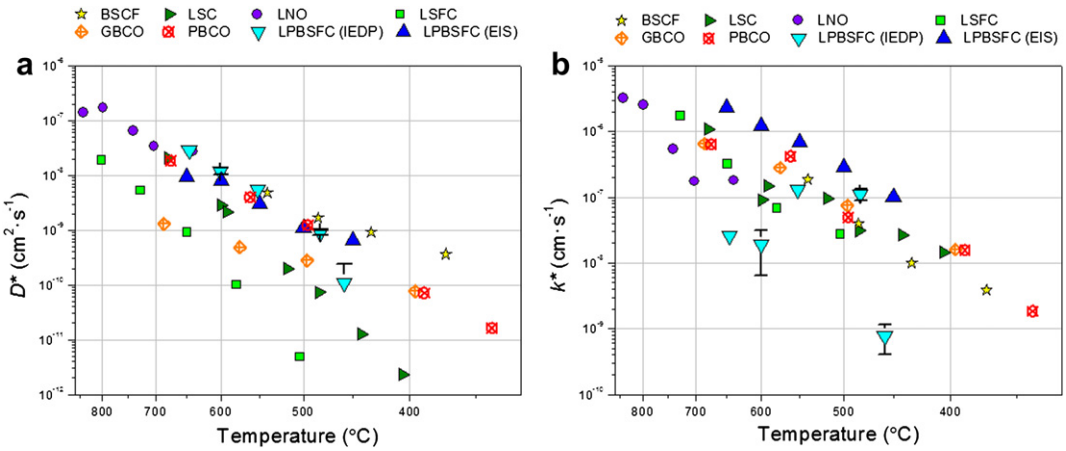

Fig. 3. Arrhenius plot of diffusion (a) and surface exchange (b) coefficients for the LPBSFC material. Values obtained from isotopic exchange experiments (this work) are shown as inverted triangles (cyan) and are compared with other IEDP data from the literature for other cathode materials: $La_{0.6}Sr_{0.4}Fe_{0.8}Co_{0.2}O_{3-\delta}$ (LSFC) [12], $Ba_{0.5}Sr_{0.5}Co_{0.8}Fe_{0.2}O_{3-\delta}$ (BSCF) [16], $La_{0.6}Sr_{0.4}CoO_{3-\delta}$ (LSC) [13], $La_2NiO_{4+\delta}$ (LNO) [14] and $GdBaCo_2O_{5+\delta}$ (GBCO) [15], and finally those obtained from EIS measurements [3] are shown as regular triangles (blue). (For interpretation of the references to colour in this figure legend, the reader is referred to the web version of this article.)

What is not known, and is quite probable, is that microstructural differences could exist and are thus though to be the most likely source of the discrepancy.

For the D values, although there is some discrepancy in the absolute values, it is much smaller than that observed for k. The activation energy for the EIS-derived D_i coefficient (1.24 eV) is close to the value calculated from the IEDP coefficients (1.41 ± 0.17 eV), as can be seen in Fig. 3a. This reinforces the conclusion that the high oxygen diffusion coefficients obtained from IEDP measurements for dense LPBSFC material are in good agreement with those obtained from EIS measurements on porous LPBSFC cathodes, given the possible errors discussed above.

The high scatter of the k^* (IEDP) coefficient values does not allow a direct comparison with all the k_i (EIS) values (Fig. 3b). Nevertheless, for the intermediate temperatures 482 and 553 °C the differences between the two sets of values are the smallest and of the same order of magnitude as those observed for the diffusion coefficients (Fig. 3a). This indicates that the LPBSFC material might show high oxygen surface exchange, as proposed earlier in Ref. [3]: where the improvement is principally ascribed to the basicity of Ba cations and the redox properties of Pr. More detailed, surface specific, experiments are being carried out to elucidate the cause of the large scatter in the LPBSFC k^* values. In addition to the parametric assumptions made for the calculation of the EIS-derived D_i and k_i coefficients, another factor affecting the comparison of the surface exchange coefficients could be the differences in the fabrication/temperature history for the IEDP and EIS samples. This could have a strong influence in the surface state and composition and, as consequence, in the oxygen surface exchange kinetics.

4. Conclusions

Oxygen tracer experiments have been carried out in order to corroborate the promising electrochemical properties for oxygen activation of the low barium-containing $La_{0.2175}Pr_{0.2175}Ba_{0.145}Sr_{0.4}Fe_{0.8}Co_{0.2}O_{3-\delta}$ perovskite previously determined by electrochemical impedance spectroscopy measurements. $^{18}O_2/^{16}O_2$ isotopic exchange has been performed on $La_{0.2175}Pr_{0.2175}Ba_{0.145}Sr_{0.4}Fe_{0.8}Co_{0.2}O_{3-\delta}$ samples at different temperatures. By fitting the normalised isotopic concentration data the oxygen diffusion and surface exchange coefficients have been obtained. Compared to the data reported for similar state-of-the-art cathode materials, the $La_{0.2175}Pr_{0.2175}Ba_{0.145}Sr_{0.4}Fe_{0.8}Co_{0.2}O_{3-\delta}$ composition presents one of the highest oxygen diffusion coefficients. In addition, these values and the corresponding activation energy of the process are in agreement with those calculated from the Gerischer parameters obtained by fitting electrochemical impedance spectroscopy data from electrode materials of the same composition.

On the other hand, the tracer surface oxygen coefficients obtained present a large scatter, the origin of which is the subject of a further in-depth study. The values obtained for two intermediate temperatures (482 °C) are comparable to those reported for other perovskite materials and they also show limited agreement with those obtained from the EIS modelling of porous LPBSFC electrodes. The surface exchange coefficients obtained from the EIS measurements are larger than those obtained by the isotopic exchange method, which can be explained by differences between real and estimated cathode microstructural parameters and thermal sample history.

In summary, the $La_{0.2175}Pr_{0.2175}Ba_{0.145}Sr_{0.4}Fe_{0.8}Co_{0.2}O_{3-\delta}$ perovskite has been shown to display high oxygen ion diffusion as determined by means of oxygen isotopic exchange measurements. The oxygen surface exchange rate show considerable scatter, but for two of the measured temperatures (482 and 553 °C) these seem to be comparable to other state-of-the-art cathode materials. These results are in agreement with previous results showing the promising electrocatalytic properties (low polarization resistance) of $La_{0.2175}Pr_{0.2175}Ba_{0.145}Sr_{0.4}Fe_{0.8}Co_{0.2}O_{3-\delta}$ electrodes. This reinforces the relevance of using the new multi-element analysis [2] for discovering new electrode materials and the suitability of the $La_{0.2175}Pr_{0.2175}Ba_{0.145}Sr_{0.4}Fe_{0.8}Co_{0.2}O_{3-\delta}$ material for IT-SOFC cathode and oxygen membrane applications.

Acknowledgements

Funding from the Universitat Politècnica de València (grants FPI-UPV-2007-06 and PAID-00-10) and Spanish Government (grant ENE2011-24761) is kindly acknowledged. The research leading to these results has received funding from the European Union Seventh Framework Programme (FP7/2007-2013) under grant agreement n°: PIEF-GA-2009-252711 and from King Abdullah University of Science and Technology (KAUST) through a research grant. The authors would like to thank S. Jiménez for material and sample preparation and Dr. S. Fearn, R. Charter and S. Cook for their help with ToF-SIMS analysis.

References

[1] F. Tietz, H.-P. Buchkremer, D. Stöver, Solid State Ionics 152–153 (2002) 373.
[2] J.M. Serra, V.B. Vert, ChemSusChem 2 (2009) 957.
[3] J.M. Serra, V.B. Vert, J. Electrochem. Soc. 157 (2010) B1349.
[4] M.P. Pechini, Patent US 3 330 697 (1967).
[5] R.A. De Souza, J. Zehnpfenning, M. Martin, J. Maier, Solid State Ionics 176 (2005) 1465.
[6] J.A. Kilner, B.C.H. Steele, L. Ilkov, Solid State Ionics 12 (1984) 89.
[7] R.J. Chater, S. Carter, J.A. Kilner, B.C.H. Steele, Solid State Ionics 53–56 (1992) 859.
[8] RH.E. van Doorna, I.C. Fullarton, R.A. de Souza, J.A. Kilner, HJ.M. Bouwmeester, A.J. Burggraaf, Solid State Ionics 96 (1997) 1.
[9] J.M. Serra, V.B. Vert, O. Büchler, W.A. Meulenberg, H.P. Buchkremer, Chem. Mater. 20 (2008) 3867.
[10] J. Crank, Mathematics of Diffusion, second ed. Oxford University Press, Oxford, 1975, pp. 36.
[11] D.R. Killoran, J. Electrochem. Soc. 109 (1962) 170.
[12] S.J. Benson, PhD thesis, Department of Materials, Imperial College, London (1999).
[13] A.V. Berenov, A. Atkinson, J.A. Kilner, E. Bucher, W. Sitte, Solid State Ionics 181 (2010) 819.
[14] S.J. Skinner, J.A. Kilner, Solid State Ionics 135 (2000) 709.
[15] A. Tarancón, S.J. Skinner, R.J. Chater, F. Hernández-Ramírez, J.A. Kilner, J. Mater. Chem. 17 (2007) 3175.
[16] A. Berenov, A. Atkinson, J. A. Kilner, E. Bucher, W. Sitte, Proceedings of the 8th European Fuel Cell Forum, Lucerne, Switzerland, 2008.
[17] M. Burriel, J. Peña-Martínez, R.J. Chater, S. Fearn, A.V. Berenov, S.J. Skinner, J.A. Kilner, Chem. Mater. 24 (2012) 613–621. doi:10.1021/cm203502s.
[18] R. Merkle, Y.A. Mastrikov, E.A. Kotomin, M.M. Kuklja, J. Maier, J. Electrochem. Soc. 159 (2012) B219.
[19] Y.L. Yang, A.J. Jacobson, Mat. Res. Soc. Symp. Proc. 548 (1998) 551.
[20] A. Leonide, B. Rüger, A. Weber, W.A. Meulenberg, E. Ivers-Tiffée, J. Electrochem. Soc. 157 (2010) B234.
[21] A. Esquirol, J.A. Kilner, N. Brandon, Solid State Ionics 175 (2004) 63.
[22] J. Maier, Solid State Ionics 112 (1998) 197.
[23] J. Maier, Solid State Ionics 135 (2000) 575.